Surface structures and phase diagram for the H/W(001) chemisorption system

R. A. Barker and P. J. Estrup

Citation: The Journal of Chemical Physics **74**, 1442 (1981); doi: 10.1063/1.441211
View online: http://dx.doi.org/10.1063/1.441211
View Table of Contents: http://scitation.aip.org/content/aip/journal/jcp/74/2?ver=pdfcov
Published by the AIP Publishing

Surface structures and phase diagram for the H/W(001) chemisorption system

R. A. Barker[a] and P. J. Estrup

Department of Physics and Department of Chemistry, Brown University, Providence, Rhode Island 02912
(Received 28 August 1980; accepted 16 September 1980)

The chemisorption of hydrogen on tungsten (001) induces displacive rearrangements ("reconstruction") of the substrate surface, depending on the temperature T and the adsorbate coverage θ. By means of LEED and other techniques, the surface phase diagram in the T–θ plane ($\theta < 0.7$, $T < 500$ K) has been studied. The predominant structure is $(\sqrt{2}\times\sqrt{2})$ which is stabilized by hydrogen in the region $\theta < 0.3$, but is transformed to an incommensurate structure at higher coverages. Adsorption below $\simeq$200 K produces no ordered phase. The LEED patterns from a terraced surface exhibit reduced symmetry and reveal the direction of the lattice distortion; the atomic displacements are found to be along $\langle 10\rangle$ for the H-induced structures, in contrast to the $\langle 11\rangle$ displacements on clean W(001). The substrate rearrangement is believed to be a major cause of the observed coverage dependence of the desorption energy and other adsorbate properties.

I. INTRODUCTION

The adsorption of hydrogen on tungsten (001) has been studied by many different techniques during the last decade. As additional data gradually have become available, the behavior of the system has appeared increasingly complex, and no model was found that could account satisfactorily for all the experimental observations.[1,2] It now seems clear that the complexity of this chemisorption system is due to the occurrence of displacive structural transformations ("reconstruction") of the substrate. It has been found that a *clean* W(001) surface rearranges to give a $(\sqrt{2}\times\sqrt{2})$ structure when the crystal is cooled below room temperature[3,4] and several structural features of this low-temperature phase have been determined.[5,6] It has also been shown that the structural changes observed during the adsorption of hydrogen involve similar rearrangements of the tungsten lattice.[7–10] Such adsorption-related changes are probably not confined to the W(001)/H system; for example, the Mo(001) surface shows the same type of behavior.[3,10,11] It appears that the transformations depend on a lowering of the surface electronic energy but the detailed mechanism is not completely understood.[12,13] One possibility is that it involves a Fermi surface instability that leads to the formation of charge density waves (CDW) coupled to a periodic lattice distortion (PLD); another possibility is that the structural changes are analogous to Jahn–Teller distortions in which case a bond model may be more useful in describing the phenomenon.

In this paper we present further data concerning the nature of the surface phases that form on W(001) at relatively low hydrogen coverage. The data are summarized in a T–θ (temperature–coverage) phase diagram, described in Sec. III. As previously reported,[7] work function measurements permit an accurate determination of the relative coverage at which characteristic changes occur in low energy electron diffraction (LEED), electron stimulated desorption (ESD) yields, and in the desorption activation energy E_d. The correlations found in this way[7] between the structural and electronic properties provide part of the evidence that the phase transformations are driven by the surface electronic energy. King and Thomas[14] have recently extended these arguments on the basis of additional detailed coverage measurements.

The new results to be reported here include LEED data for "nondegenerate" structures. For a perfect two-dimensional ($2D$) crystal the symmetry of the LEED pattern about the origin is the same as the point group symmetry of the unit mesh; however, the observed LEED patterns often have a higher symmetry because of "rotational degeneracy." For example, if the unit mesh is rectangular, it may be oriented in two equivalent ways on a fourfold symmetric substrate and the surface will therefore contain two kinds of domains, usually in equal abundance. A LEED measurement will give the sum of the intensities diffracted from these domains, and the pattern will consequently have fourfold symmetry. If for any reason one of the orientations is preferred over the other so that the rotational degeneracy is lifted, the symmetry of the LEED pattern will be reduced to twofold. A partial lifting of domain degeneracy was observed by Debe and King[5] on clean W(001), and the unit mesh symmetry of the low-temperature structure could therefore be determined. In the present study of the hydrogen-induced structures we have succeeded in obtaining completely nondegenerate patterns after a deliberate search near the edges of the ribbon-shaped samples where long and narrow terraces are likely to exist. As described in Sec. IV. the results show that, at least at some coverages, the H–$(\sqrt{2}\times\sqrt{2})$ unit has C_{2mm} symmetry and that the tungsten atom displacements are along $\langle 01\rangle$. By contrast, the atomic displacements in the clean low temperature phase are along the $\langle 11\rangle$ directions.

Among the unusual changes seen by LEED for W(001)/H is a continuous splitting of the $(\frac{1}{2}\frac{1}{2})$ beams into four

[a]Present address: Bell Laboratories, Murray Hill, N.J. 07974.

 0021-9606/81/021442-11$01.00

new beams.[15] At room temperature this splitting begins when the coverage exceeds $\theta \approx \frac{1}{3}$ monolayer but the degree of splitting depends on the temperature. We have noted earlier[7,10] the possibility that this splitting could be due to an incommensurate PLD similar to that suggested for the low-temperature phase on clean Mo(001),[3] and King and Thomas[14] have proposed structural models based on this hypothesis. On the other hand, such beam splitting can also arise from the antiphasing of domains of the (registered) $(\sqrt{2} \times \sqrt{2})$ structure. Both types of incommensurate structure are discussed in Sec. V in light of the data obtained for both ordinary and terraced W(001) surfaces. These structures are assigned a separate region in the phase diagram since their formation corresponds to a decrease in the long-range order in one direction. Increases in either T or θ eventually destroys the long-range order in both directions, producing a disordered phase.

II. EXPERIMENTAL PROCEDURES

The experimental apparatus used in these investigations consisted of an all-steel ultra-high vacuum chamber, routinely capable of reaching a base pressure of $\simeq 1 \times 10^{-10}$ Torr and equipped with a standard three grid LEED optical system. A precision sample manipulator with rotational and XYZ movements made it possible to investigate the edges of the crystal with a finely focused electron beam. The sample holder was constructed so that the sample could be either ohmically heated or cooled to near 120 K with liquid nitrogen, and heavy molybdenum clamps allowed the sample to reach well below room temperature in about 3 to 5 s after a flash to 2500 K. This was useful in establishing the low-temperature properties of the clean surfaces and allowed adsorption experiments to begin within seconds of heating. In most experiments the sample temperature was monitored with a W–Re5%/W–Re26% thermocouple that was spot welded to the rear of the sample. This particular thermocouple was chosen because the emf is nearly linear with temperature and is large below room temperature. Control of the sample temperature was accomplished by the use of a pulsed heating circuit that could ramp the temperature either up or down, linearly with time, or hold it constant to within a few degrees. The pulsed heater served as a controllable heat source and the molybdenum clamps as a large heat sink. This combination allowed the temperature to be varied through the entire temperature range of interest as often as every 2 or 3 s. A single flash to 2500 K was usually sufficient to clean the sample although periodic oxygen treatments were required.

LEED intensities were measured by monitoring the spot brightness on the fluorescent screen, using a specially built spot photometer containing a beam splitter and a photomultiplier tube. Intensity measurements could be made as a function of incident electron energy, temperature, or coverage. For intensity vs temperature measurements the signal from the spot photometer was stored in a gating circuit when the heating pulse was in an "off" state to eliminate the effects of electric and magnetic fields on the electron beam.

The work function change $\Delta\phi$ was measured by means of the retarding potential method. The diode formed by the LEED electron gun and the sample was kept on the halfway point of its current vs voltage curve with an simple feedback circuit. This method[16] allowed $\Delta\phi$ to be measured continuously as a function of time within ± 5 mV. Since the work function for hydrogen on W(001) is nearly linear with the coverage,[15,17] $\Delta\phi$ can be used as a convenient monitor of surface hydrogen density. The saturation coverage of hydrogen is near two atomic monolayers[18] ($\theta = 2$), which gives a work function change of 0.95 eV[15,17]; thus, the relative coverage can be monitored to within a few hundredths of a monolayer.

The present vacuum system could be used without alteration for simultaneous measurements of LEED, Auger electron spectroscopy (AES), $\Delta\phi$, and ESD.[19] The ability to monitor $\Delta\phi$ continuously made it possible also to obtain adsorption isobars.[7] These were measured by first heating the sample to a temperature that prevented hydrogen adsorption and then monitoring $\Delta\phi$ (and hence the coverage) and temperature as the sample was slowly cooled. The detailed results of these experiments will be reported elsewhere.[20]

Of particular importance to this study was the preparation of the sample, which consisted of a thin metal ribbon measuring about 0.005 in. $\times$ 0.2 in. $\times$ 1.3 in. The sample was cut to rectangular shape with the edges along the $\langle 01 \rangle$ directions. The subsequent mechanical and electrochemical polishing procedures produced terraces along the edges through a rounding of the corners, as illustrated in Fig. 1. After mounting of the sample in the LEED chamber, examination showed effects of terraces up and down the entire length of both sides of the sample. In some of the LEED patterns

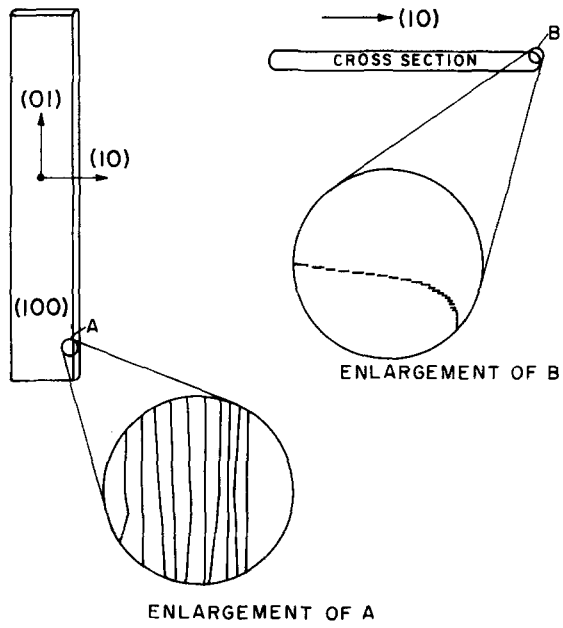

FIG. 1. Sketch of the tungsten (001) ribbon, illustrating the terraced regions at the edges of the sample.

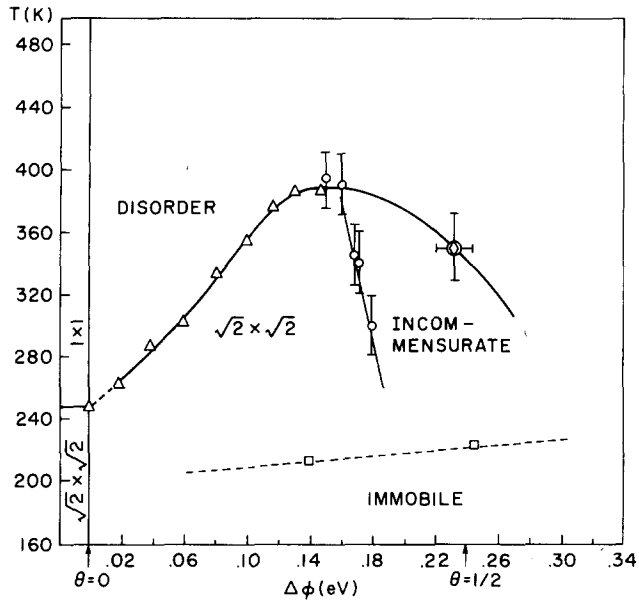

FIG. 2. Phase diagram for H/W(001) showing the regions in the $T-\theta$ plane where the different structures are stable. The observed phases of clean W(001) are shown to the left of $\theta = 0$. The "incommensurate" phase is characterized by split $\frac{1}{2}\frac{1}{2}$ LEED beams. No superstructures are produced by H_2 adsorption below ≈ 200 K, i.e., in the "immobile" region.

the integral order beams were slightly elongated in the ⟨10⟩ direction at certain voltages. This indicates that the terrace widths (perpendicular to the length of the sample) are of the order of 10^2 Å.

III. PHASE DIAGRAM

Complex changes take place in the tungsten surface in the early stages of adsorption. The structures formed are a function of temperature as well as coverage; thus, it is appropriate to present the LEED results by means of a phase diagram. To obtain the diagram shown in Fig. 2, the surface structures were recorded for values of θ, T, and gas phase pressures P at which both adsorption and desorption can be neglected, so that the surface can be considered a closed system.[10] The absence of hysteresis effects was evidence that the surface had reached equilibrium in each observation. Work function data were used as a measure of the coverage. The point at which $\theta = \frac{1}{2}$ has been marked with an arrow and was located by assuming a saturation value of $\theta_s = 2$. The regions to the left of $\theta = 0$ correspond to the *clean* surface phases.

The diffraction patterns that occur while moving horizontally from left to right in the phase diagram at room temperature are shown in Fig. 3, beginning with the clean surface [Fig. 3(a)]. Initially, the half-order beams are somewhat broadened but eventually they sharpen to give the pattern in Fig. 3(b), which is characteristic of the ordered $(\sqrt{2}\times\sqrt{2})$ region in the phase diagram. The triangular points that separate this region from the disordered region above were obtained from a family of intensity vs temperature curves at several values of θ (Fig. 4). The critical temperature is defined somewhat arbitrarily by the solid line in Fig. 4; however, this choice is consistent with the data given below for the beam broadening.

The intensity of the extra beams rises nearly linearly with coverage until $\theta \approx \frac{1}{3}$ at which point they split cleanly into four new beams [Fig. 3(c)]. The intensity (the total of the four beams) then begins to diminish while the new extra beams travel smoothly away from the half-order positions along [10] and [01]. This transition to the "split beam" phase is marked by the straight line in Fig. 2 to the right of the $(\sqrt{2}\times\sqrt{2})$ region. The points defining this line were obtained by measuring the coverage and temperature where the beams were first observably split and then correcting for the fact that the LEED beams have finite width due to the limited experimental resolution. It should be noted that the splitting of the half-order beams is also a function of temperature, as indicated by the finite slope of the line. The temperature dependence has been measured and is presented in Sec. V. The temperature could be raised and lowered by 200 K every 2 s (Sec. II), and the split beams were observed to move into and back away from the half-order position with the same period. The fourfold splitting actually arises from regions of twofold symmetric structures, which give only twofold beam splitting along either [01] or [10]. This point is discussed in greater detail below. The splitting is ascribed to the formation of incommensurate structures, and the region in the phase diagram is labeled accordingly.

The split beams remain sharp over a range of θ but eventually, as the coverage is increased, the beams begin to streak in a direction perpendicular to their direction of travel [see Fig. 3(d)], signifying a loss of long-range order in the remaining direction. This transition is marked in the phase diagram by the boundary between the incommensurate and disordered regions. These streaked patterns [Fig. 3(d)] are remarkably curved at somewhat lower temperatures [Fig. 3(e)]. The detailed shape of the boundary in the phase diagram is not known exactly and it has been drawn in part from visual observations. The weaker patterns that develop at still higher coverages[15] are not included in the diagram and will not be discussed here.

The nearly horizontal line in the diagram at about 200 K represents an irreversible change and, strictly speaking, does not belong in a phase diagram. If adsorption proceeds at a temperature below this line, the usual sequence of diffraction patterns is not observed. At these temperatures the clean surface has already rearranged to a $(\sqrt{2}\times\sqrt{2})$ phase and the only effect of hydrogen is to reduce the half-order beam intensities and to increase the background scattering. When the sample is warmed to a temperature above the dashed line, the diffraction pattern corresponding to that particular temperature and hydrogen coverage appears and remains present when the sample is again cooled below the dashed line. Further adsorption on the cold surface does not

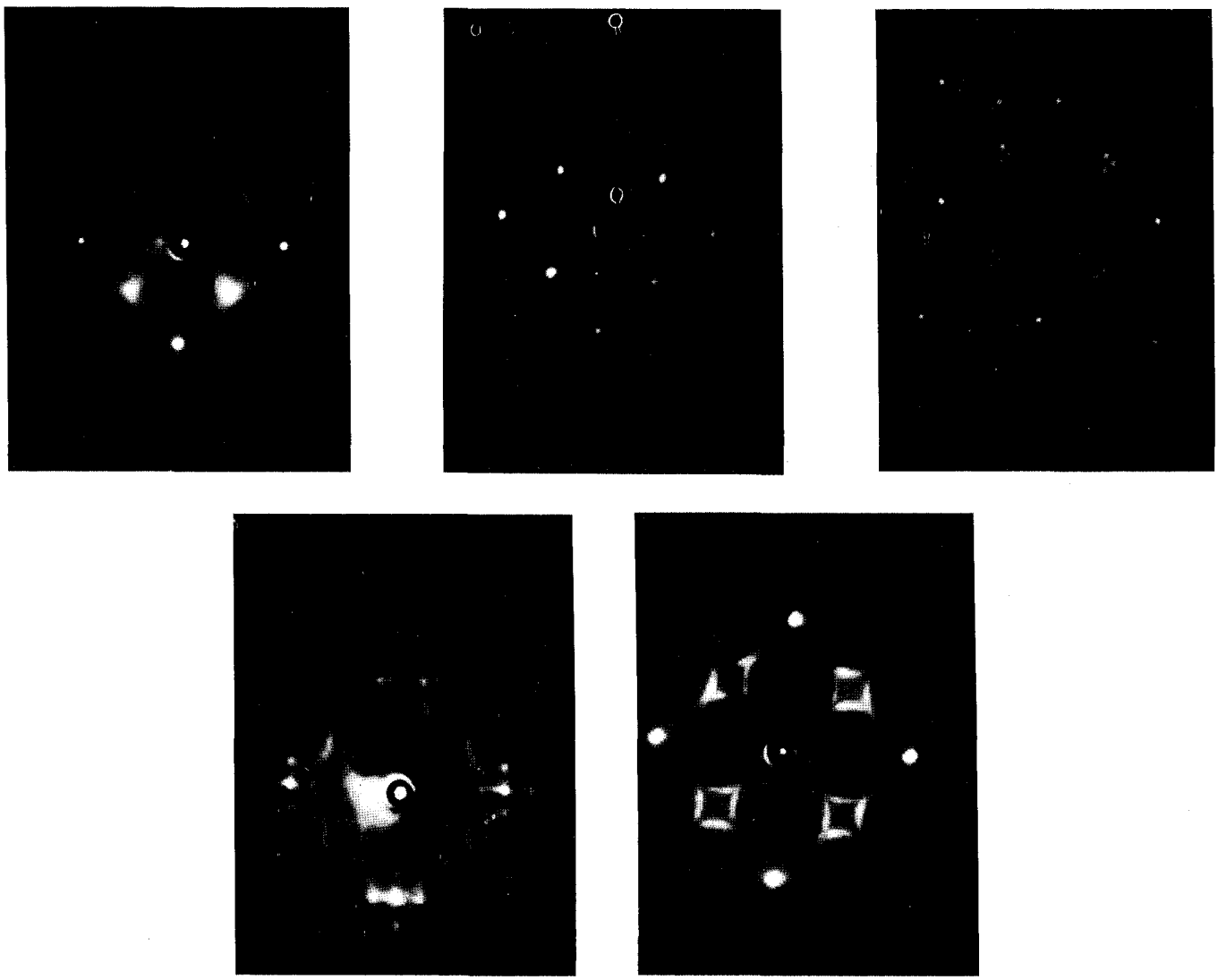

FIG. 3. LEED patterns produced by hydrogen adsorption at room temperature. Electron beam energy 45 eV. (a) Clean W(001), showing remnants of the low-temperature $(\sqrt{2}\times\sqrt{2})$ phase. (b) $(\sqrt{2}\times\sqrt{2})$ pattern. (c) "Split" $(\sqrt{2}\times\sqrt{2})$ pattern, corresponding to an incommensurate structure. (d) Streaky pattern, corresponding to loss of long-range order in both directions. (e) Streaky pattern produced at somewhat lower temperature showing distinctly curved diffraction features.

produce the changes expected at room temperature (i.e., increased beam splitting) until the sample is again warmed above the dashed line. This effect is demonstrated in Fig. 5, where the half-order beam intensity is plotted vs T for two different coverages. Adsorption was carried out at low T and then the sample was heated. The upper curve was recorded at a coverage where the beams do not split and the $(\frac{1}{2}\frac{1}{2})$ beam intensity is seen to increase as the H–$(\sqrt{2}\times\sqrt{2})$ structure is formed. The lower curve was taken at a coverage above the beam splitting so that, as the surface is heated, intensity is removed from the $(\frac{1}{2}\frac{1}{2})$ position and the recorded intensity drops nearly to zero. These effects suggest that at low temperature the periodic lattice distortions are hindered, perhaps because the adsorbate is nearly immobile.

The full width at half-maximum (FWHM) of the $(\frac{1}{2}\frac{1}{2})$ beam is shown in Fig. 6. The first data point, at zero coverage, is due to the broad and weak diffraction feature remaining at 400 K from the clean $(\sqrt{2}\times\sqrt{2})$ structure. An outline of the H–$(\sqrt{2}\times\sqrt{2})$ region of the phase diagram (Fig. 2) has been superimposed on this figure. The horizontal dashed line corresponds to the T and θ values for which the FWHM data were collected. It is seen that the gradual drop in the FWHM ceases at a coverage that corresponds to the boundary between the disordered and ordered phases. A similar behavior of the width of the superlattice reflections has been seen for phase transitions in the O/W(110)[21] and O/Ni(111)[22] systems, and the analogous $3D$ phenomenon has been studied extensively, e.g., in alloys.[23] In their study of H/W(001) King and Thomas[14] reported that the FWHM rapidly decreases and levels off at low coverage. This is not surprising, since their data were taken at a lower temperature and, according to the phase diagram (Fig. 2), the ordered phase is then produced at a much lower coverage.

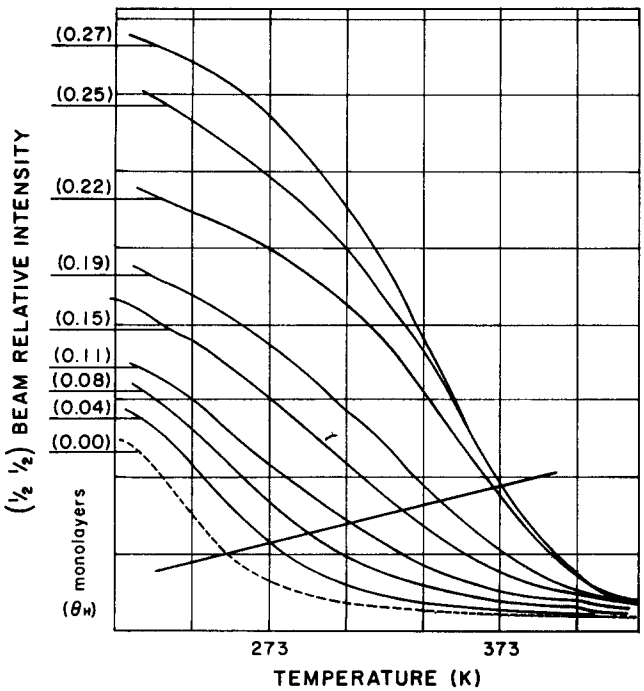

FIG. 4. Intensity of the $\frac{1}{2}\frac{1}{2}$ beam as a function of temperature at several coverages. The coverage in monolayers is shown on the left. The lowest curve (broken line) is for the clean surface. The heavy black line shows the choice ot T_c.

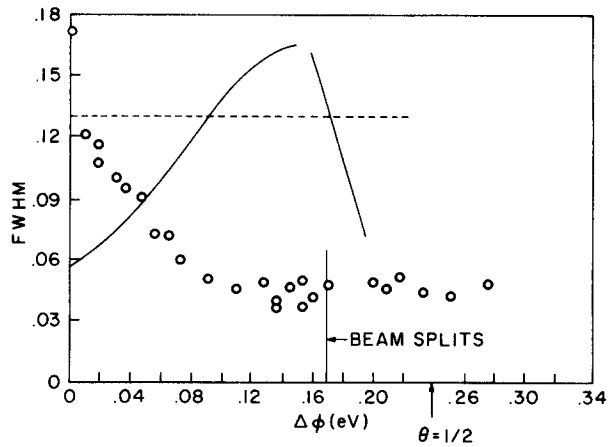

FIG. 6. Full width at half-maximum of the $\frac{1}{2}\frac{1}{2}$ beam as a function of coverage, in units of $2\pi/a$ (the reciprocal lattice parameter). The split beams were scanned in a direction parallel to their travel so that FWHM is the width of the streaks [cf. Fig. 3(d)]. The relevant regions of the phase diagram have been superimposed for comparison. The dashed line indicates the values of T and θ for which the data were collected. The FWHM begins to level off where this dashed line crosses into the ordered $(\sqrt{2}\times\sqrt{2})$ region.

No thermodynamic data are obtained by the methods used here and the available structural information does not provide a complete characterization of the phase

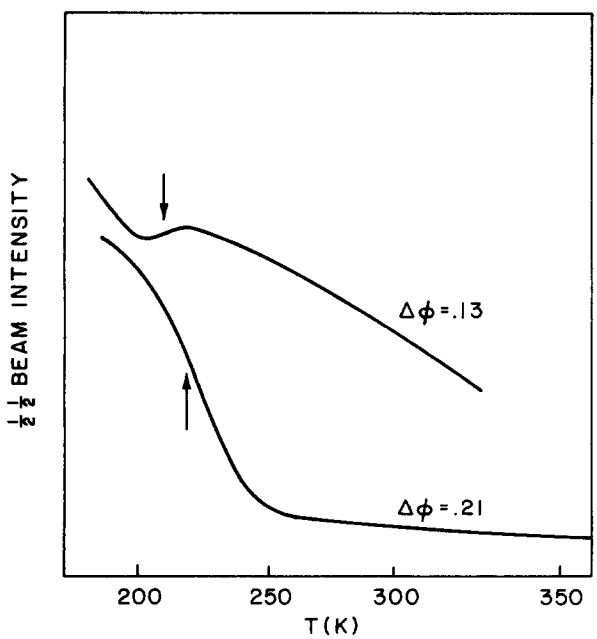

FIG. 5. $\frac{1}{2}\frac{1}{2}$ beam intensity vs temperature showing the irreversible changes as the mobility increases. The upper curve ($\Delta\phi=0.13$, $\theta=0.25$) represents a change to the ordered $(\sqrt{2}\times\sqrt{2})$ and the intensity increases. The lower curve ($\Delta\phi=0.21$, $\theta\simeq 0.4$) represents a change to the incommensurate phase and the intensity of the split $\frac{1}{2}\frac{1}{2}$ beam decreases. The arrows correspond to the boundary of the "immobile" region in Fig. 2.

changes. The intensity measurements in Fig. 4 indicate that the nature of the $(\sqrt{2}\times\sqrt{2})\rightarrow(1\times1)$ transformation is the same for the clean and for the adsorbate covered surface. The decrease of $I(\frac{1}{2}\frac{1}{2})$ together with the beam broadening suggest a continuous phase transition in which the magnitude of the displacements and their long-range correlations gradually decrease as the temperature is raised. A PLD/CDW mechanism may account for this general behavior and, as shown by Lau and Ying,[24] the stabilizing effect of hydrogen can be explained by including the interaction of the adatoms with the periodically distorted substrate.

The interpretation of $I(\frac{1}{2}\frac{1}{2})$ vs T in terms of a decreasing distortion amplitude and critical scattering agrees with earlier suggestions[3] but is not the only explanation proposed. Debe and King[25] report that the $(\sqrt{2}\times\sqrt{2})\rightarrow(1\times1)$ transition on clean W(001) produces a break in the slope of $I(T)$ for several integral order LEED beams, including the (00) beam. This break, assumed to coincide with the transition temperature, is taken as evidence that the phase change is not continuous but involves coexisting $(\sqrt{2}\times\sqrt{2})$ and (1×1) structures. The decreasing $I(\frac{1}{2}\frac{1}{2})$ vs T curve should therefore measure the changing relative abundance of these two phases. However, there would seem to be difficulties with this argument: (1) The breaks in the $I(T)$ plots are reported[25] to occur at different temperatures depending on the diffraction spot and the electron energy, (2) curves without any break or with changes in slope in the opposite direction were seen in the present study and in that by Heilmann *et al.*,[26] and (3) at least in the kinematical approximation the displacive phase transition will not affect the value of the $2D$ structure factor for the (00) reflection; hence, as the crystal cools, the intensity of the $(\frac{1}{2}\frac{1}{2})$ beams will increase at the expense of all the inte-

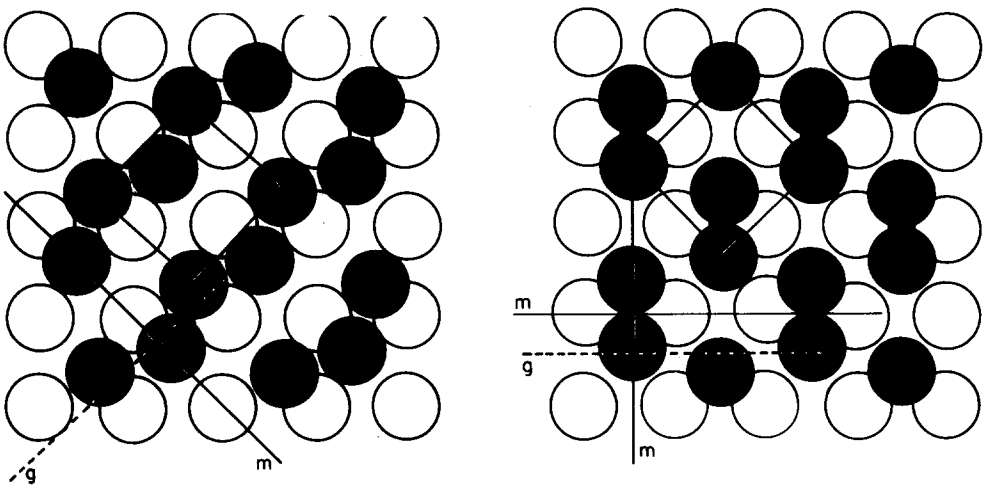

FIG. 7. (a) Model of the low-temperature W(001) structure, showing the $(\sqrt{2}\times\sqrt{2})$ unit mesh and the glide and mirror planes. The filled circles represent the top layer; the open circles, the second layer. (b) Model of the hydrogen-induced $(\sqrt{2}\times\sqrt{2})$ structure near $\theta = \frac{1}{3}$. The filled circles represent the top layers of W atom. The H atoms are not shown but are located preferentially on top of the W dimers. In both figures the displacements have been exaggerated for clarity.

gral order beams *except* the (00). A more plausible explanation of the temperature dependence of this beam would seem to be that the phonon spectrum and therefore the effective Debye–Waller factor changes as the surface rearranges.[26]

IV. SYMMETRY OF SURFACE STRUCTURES

A. $(\sqrt{2}\times\sqrt{2})$ structures

With the samples used in the present study, no LEED patterns with less than fourfold symmetry were seen for the clean surface, not even on the terraced regions. This is consistent with the model for the rearranged surface shown in Fig. 7(a); the $(\sqrt{2}\times\sqrt{2})$ unit is due to a periodic lattice distortion (PLD) consisting of a displacement wave parallel to either [11] or [1$\bar{1}$]. Two rotational domains are possible and since they will be affected equally by defects parallel to [01], no removal of the degeneracy is expected. However, a sample used by Debe and King[5] showed a preference for one of the two orientations, and from the resulting LEED intensity variation it is possible to deduce the existence of a mirror plane (m) and a glide plane (g) in the structure, as depicted in Fig. 7(a). This symmetry (P_{2mg}) for a $(\sqrt{2}\times\sqrt{2})$ structure determines uniquely the direction of atomic displacements in the plane of the surface.[5] LEED intensity calculations have confirmed the model[6,27] and lattice dynamical calculations have rationalized the preference for this particular distortion (which is equivalent to a frozen-in M_5 phonon).[28]

The evidence that the hydrogen-induced structures also involve displacements of the W atoms come from LEED results[6] and, more recently, ion scattering measurements[9] and electron energy loss spectra.[8] There are strong similarities between the clean $(\sqrt{2}\times\sqrt{2})$ and the H–$(\sqrt{2}\times\sqrt{2})$ structures and in both cases the lateral displacements are $\gtrsim 0.2$ Å,[6,8,9] but certain differences exist that appear to eliminate the possibility that the hydrogen-induced structure is a clean $(\sqrt{2}\times\sqrt{2})$ structure [Fig. 7(a)] with the hydrogen added on top. These differences include subtle changes in the LEED beam intensity vs voltage [$I(V)$] curves,[25,6] and a change of symmetry at a particular hydrogen density. The arguments presented below lead to the model for the H–$(\sqrt{2}\times\sqrt{2})$ structure shown in Fig. 7(b); it has space group symmetry C_{2mm}.

The diffraction patterns from terraced surfaces with the electron beam at normal incidence are different from those observed on the normal surface. When the half-order beams split, two features in the diffraction pattern have become twofold symmetric. First, as shown in Fig. 8(a), the spots have split only in the [01] direction, which corresponds to the length of the terraces. Second, the pattern, i.e., the intensity variation of the (split) half-order beams throughout reciprocal space [Fig. 8(c)], is no longer fourfold symmetric but has mirror lines parallel to [10] and [01] and an absence of such lines parallel to [1$\bar{1}$] and [11]. This is most easily seen by comparing the strong $(\frac{1}{2}\frac{3}{2})$ beam to the much weaker $(\frac{3}{2}\frac{1}{2})$ beam. These symmetry elements identify the two-dimensional space group symmetry of the surface as C_{2mm}. It is assumed that the structure can be described by a $(\sqrt{2}\times\sqrt{2})$ unit cell, i.e., that the perturbations producing a very small splitting can be ignored for the present purpose. The only displacement that produces the correct symmetry in the diffraction pattern is in the ⟨01⟩ directions and it leads to the structure shown in Fig. 7(b), which has mirror lines along [10] and both mirror and glide lines along [01]. In this coverage range the in-plane W atom displacements produce pairs of atoms ("dimers") that are pinched together along [01], as in Fig. 7(b). The model is consistent with the ELS study by Barnes and Willis[8] which shows the H atoms to be located on the twofold (bridged) sites provided by the dimers. However, due to their low scattering power, the H atoms contribute negligibly to the LEED intensity.[6,10] On the normal surface there exists an equivalent structure rotated 90° with respect to the one shown and, once again, when equal numbers of the two kinds are present, the LEED pattern is fourfold symmetric.

The switch in the direction of the metal atom displacements from ⟨11⟩ [Fig. 7(a)] to ⟨10⟩ [Fig. 7(b)] is an interesting transition that is also observed on Mo(001).[11] It can be understood by considering the so-called cubic anisotropy term in the free energy,[24,29] and the magnitude and sign of this term depends on the H–W interaction. The switch appears to occur at very low coverage

since the LEED asymmetry associated with the clean $(\sqrt{2}\times\sqrt{2})$ was seen to disappear at small hydrogen exposures.[5]

As in Fig. 7(a), the model in Fig. 7(b) depicts only the components of displacement in the plane of the surface. Recent field–ion microscopy (FIM) results[30] have been interpreted to mean that the displacements on clean W(001) have a perpendicular component, at least under the high-field conditions of these experiments, but the LEED patterns give no information about this component. It should also be noted that the ion-scattering experiments by Stensgaard and Feldman[9] suggest that only half of the top layer tungsten atoms have been displaced from their regular positions; this would imply that in Fig. 7(b) the top layer (the filled circles) should be shifted with respect to the second layer.

B. Domain selection

The surface morphology appears to be the determining factor in any removal of domain degeneracy. In particular, steps or terraces can lead to the preferential selection of one of the possible domain orientations. The results for W(001) suggest that terraces that can lift the degeneracy of the clean $(\sqrt{2}\times\sqrt{2})$ do not similarly affect the H–$(\sqrt{2}\times\sqrt{2})$ and *vice versa*. Thus, the samples that give twofold symmetric LEED patterns for the clean $(\sqrt{2}\times\sqrt{2})$ produce fourfold patterns for H–$(\sqrt{2}\times\sqrt{2})$.[5] On the other hand, the samples used in the present study give fourfold patterns for clean $(\sqrt{2}\times\sqrt{2})$ and twofold patterns for H–$(\sqrt{2}\times\sqrt{2})$. The selectivity in the latter case can be related to the external sample shape (Fig. 1); the uniformly rounded edges consist of terraces fairly accurately aligned along ⟨10⟩. Therefore, the rotational domains of the clean $(\sqrt{2}\times\sqrt{2})$ are expected to be degenerate, but the domains of H–$(\sqrt{2}\times\sqrt{2})$ are not.

If the switch from ⟨11⟩ to ⟨10⟩ (Fig. 7) occurs at low hydrogen exposure, the domain selection for H–$(\sqrt{2}\times\sqrt{2})$ must involve a change from a surface containing both [10] and [01] domains to a surface with only one of these. The progress of this domain conversion can be studied by monitoring the intensities of the $(\frac{1}{2}\frac{3}{2})$ and $(\frac{3}{2}\frac{1}{2})$ beams in Figs. 8(b) and 8(c). As shown in Fig. 9, the two beams have equal intensity at low coverage, but at $\theta \gtrsim \frac{1}{4}$ the intensity of the $(\frac{1}{2}\frac{3}{2})$ beam increases more rapidly at the expense of the $(\frac{3}{2}\frac{1}{2})$ beam. At a somewhat higher coverage the $(\frac{1}{2}\frac{3}{2})$ beam is an order of magnitude stronger than the $(\frac{3}{2}\frac{1}{2})$ beam and the pattern has become clearly twofold symmetric. The transition appears to

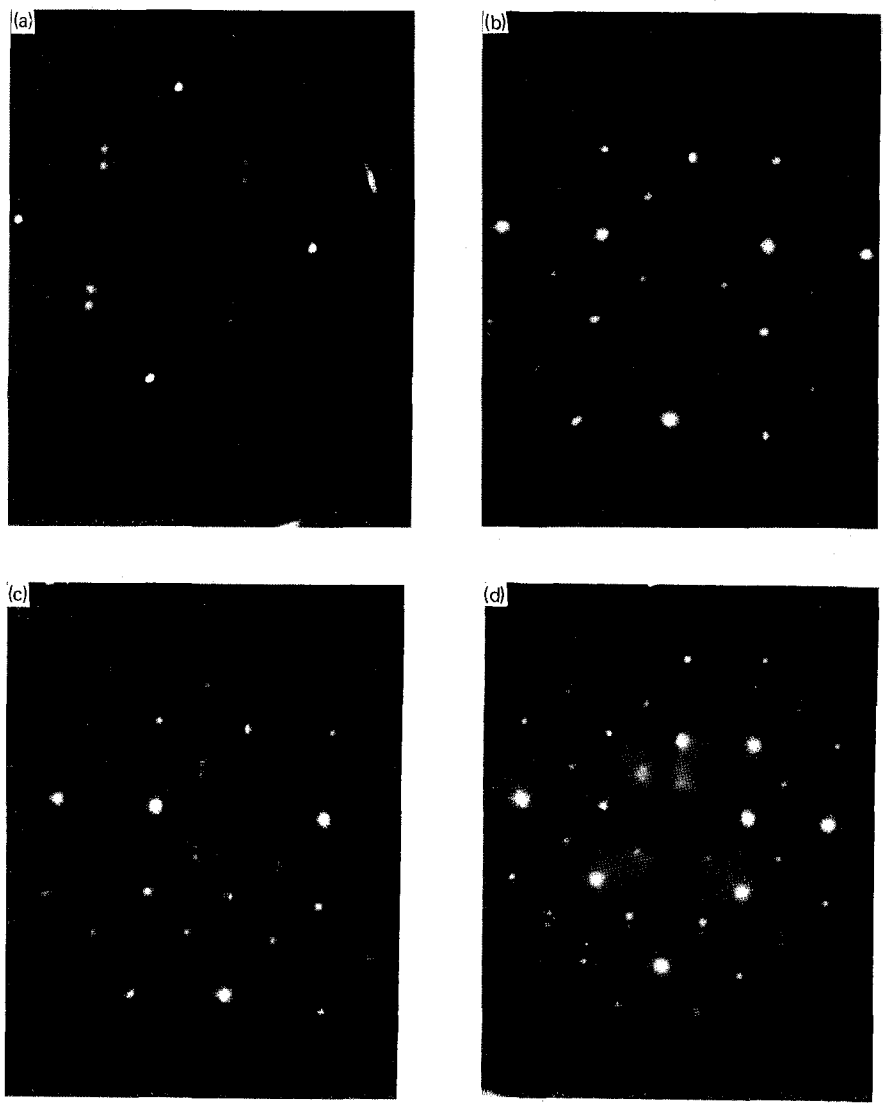

FIG. 8. LEED patterns from terraced surface. (a) Twofold splitting of the $\frac{1}{2}\frac{1}{2}$ beam along [01]. Beam energy 45 eV. (b) Pattern showing the intensity variation just before the beam splitting. Note the presence of both the $(\frac{3}{2}\frac{1}{2})$ and $(\frac{1}{2}\frac{3}{2})$ beams. Beam energy 109 eV. (c) Pattern produced by additional adsorption on (b) to split the half-order beams. Note the absence of $(\frac{3}{2}\frac{1}{2})$ and the presence of $(\frac{1}{2}\frac{3}{2})$. Beam energy 109 eV. (d) Pattern from the *center* of the sample showing the intensity variation of the split pairs in reciprocal space. Two rotational domains are present. Beam energy 158 eV.

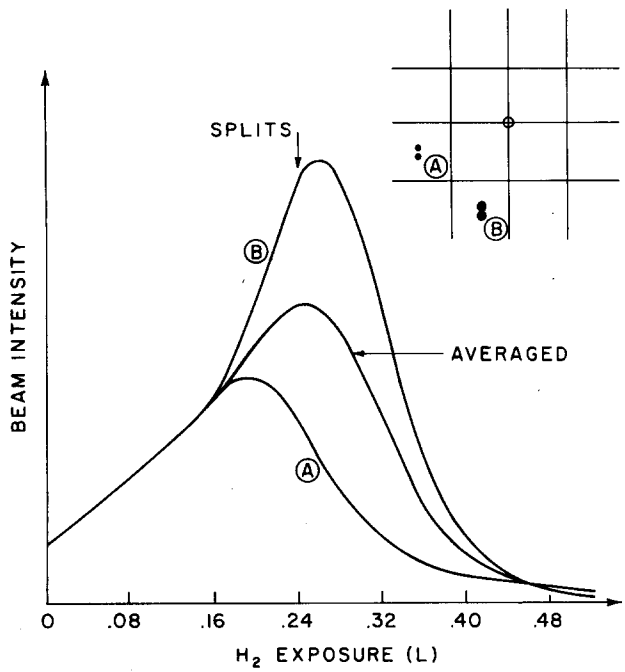

FIG. 9. Intensity of the $(\frac{3}{2}\frac{1}{2})$ (A) and the $(\frac{1}{2}\frac{3}{2})$ (B) beams from a terraced surface, as a function of coverage, showing the conversion from two to one rotational domain. The center curve is the numerical average of (A) and (B) and is similar to the intensity seen on the center of the sample. The inset (upper right) shows the position of the beams in the LEED pattern.

begin slightly before any beam splitting can be observed. The middle curve in Fig. 9 is the numerical average of the two experimental curves and is similar to the intensity measured at the center of the sample where the presence of both rotational domains averages the intensities. The reason that the [01] domains are preferred on the terraces is presumably that the edges favor the corresponding direction of the W atom displacements. This effect may become important when the coverage is sufficiently high so that the H–$(\sqrt{2}\times\sqrt{2})$ structure must extend close to the edges.

The intensity variation of the extra beams across the LEED pattern may reveal whether [10] or [01] domains are selected by the sample. Let K and K_0 represent the wave vectors for the diffracted and incident beam, respectively, and let d denote the displacement of a W atom. Then the kinematical intensity of an extra $(\frac{1}{2}m_1\,\frac{1}{2}m_2)$ spot from the 2*D* crystal in Fig. 7(b) obeys the relation

$$I(\mathbf{k}) \propto \sin^2(\mathbf{k}\cdot\mathbf{d}) , \tag{1}$$

where $\mathbf{k}=\mathbf{K}-\mathbf{K}_0=\frac{1}{2}m_1\mathbf{a}^*+\frac{1}{2}m_2\mathbf{b}^*$, and $\mathbf{a}^*$ and $\mathbf{b}^*$ are the reciprocal lattice vectors of the undistorted lattice. If $\mathbf{d}_s$, the lateral component of d, is parallel to [01], the intensity will depend on m_1 but not on m_2. Since d_s is small, the spot intensity should increase for the first several values of m_1. The corresponding dependence on m_2 is expected if $\mathbf{d}_s$ is along [10]. The (dynamical) LEED intensity should show the same qualitative behavior when an average over the beam energy is made. The observed trend in the LEED pattern is for the intensity to increase with m_1, thus implying that the atomic displacement is along [01], i.e., parallel to the terrace edge. The intensity in the quadrants nearest to the (00) beam does not fit into this trend, however, perhaps because the backscattering is especially strong in the normal direction.

C. Beam splitting and 2*D* symmetry

The simplest structural perturbation that can split the $(\frac{1}{2}\frac{1}{2})$ beam is a periodic lattice distortion (PLD) having the form of a single harmonic wave [Fig. 10(a)]:

$$\mathbf{r}_j=\mathbf{r}_{0j}+\mathbf{d}\sin(\mathbf{q}\cdot\mathbf{r}_{0j}+\delta) . \tag{2}$$

$\mathbf{r}_{0j}$ is the position of the jth atom in the undistorted lattice and the second term describes the direction and magnitude of the displacement, q being the wave vector of the distortion and δ the phase. The diffracted beams from this structure will occur for[3,10,31]

$$\mathbf{k}=\mathbf{G}\pm n\mathbf{q} , \tag{3}$$

where n is an integer, G is a reciprocal vector of the undistorted lattice, i.e., $\mathbf{G}=l_1\mathbf{a}^*+l_2\mathbf{b}^*$, and, as before, $a^*=b^*=2\pi/a$, where a is the lattice parameter of tungsten. When $\mathbf{q}=(\pi/a,\pi/a)$ the surface structure is $(\sqrt{2}\times\sqrt{2})$. In general, each integral order beam has satellites at $\pm\mathbf{q}$, $\pm2\mathbf{q}$, etc. The kinematical intensity of the nth satellite is[10,31]

$$I_n \propto J_n^2(\mathbf{k}\cdot\mathbf{d}) , \tag{4}$$

where J_n is the nth order Bessel function. Since I_n decreases rapidly with n, only the $n=1$ satellite is expected to be strong. It is seen that the translation vector for the superlattice produced by the PLD, and hence the direction of the splitting, is determined by q, that the intensity variation across the diffraction pattern depends on $\mathbf{k}\cdot\mathbf{d}$, and that the average intensity of a given spot will increase with d.

The $(\frac{1}{2}\frac{1}{2})$ beam splitting corresponds to a change from $\mathbf{q}=(\pi/a,\pi/a)$ to $\mathbf{q}=[(1-\Delta)(\pi/a),\pi/a]$. The resulting difference in k is small and any major change in I must

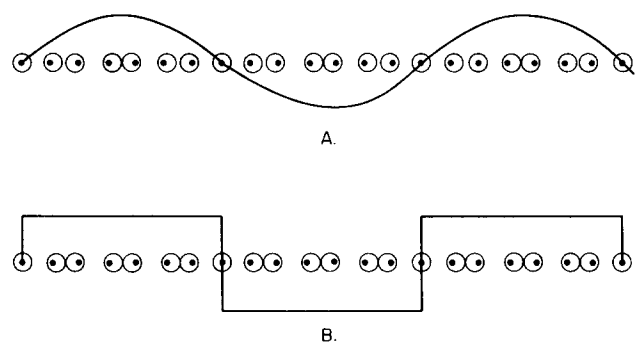

FIG. 10. Modulated 1*D* structures. (A) Pure harmonic PLD. The structure is produced by the distortion wave $\sin(q_1 n a)$, where a is the lattice parameter and n an integer. For purposes of illustration a commensurate structure is shown with $q_1=\frac{3}{7}(2\pi/a)$. Since $\sin(q_1 n a)=(-1)^{n+1}\sin(q_2 n a)$, where $q_2=\pi/a-q_1=\frac{1}{14}(2\pi/a)$, the structure may also be viewed as a dimerized crystal modulated by a distortion with wavelength $\lambda=14a$. (B) Antiphase domain structure. The structure is produced by making the modulation a square wave. As in (A), the superperiod is $14a$.

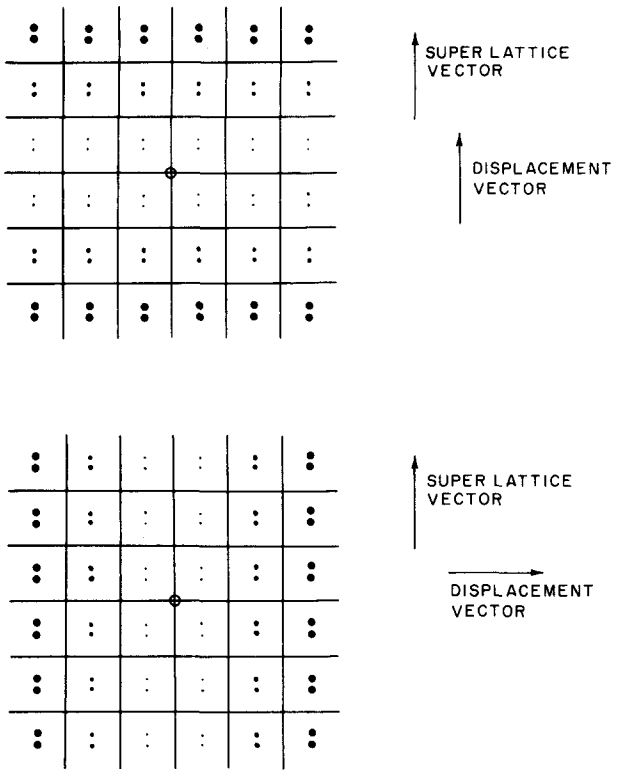

FIG. 11. Expected intensity variation of the split $\frac{1}{2}\frac{1}{2}$ beams in reciprocal space for (a) a structure having the displacement vector parallel to the superlattice vector, and (b) a structure having the displacement vector perpendicular to the superlattice vector.

therefore be due to changes in **d**. The initial intensity changes shown in Fig. 9 are therefore not caused by the new periodicity but by the domain selection described above in which **d** changes direction.

If the PLD contains higher harmonics, corresponding to $q' = mq$ (m = integer), the diffraction beams occur for

$$\mathbf{k} = \mathbf{G} + mn\mathbf{q} \ . \tag{5}$$

No new extra spots will appear, and the only change is in the relative intensity of the satellites. It should be noted that *antiphase domain structures* therefore can be described in the same way, since the antiphasing may be viewed as a distortion by a square wave [Fig. 10(b)]. In the equivalent antiphase domain description,[14,32,33] the superperiod is the distance between domain boundaries. If these are parallel to [10], the beams will split along [01], and if the boundaries run parallel to both [10] and [01] and cross each other, the beams will split in the ⟨11⟩ directions.[34] For H/W(001) the $(\frac{1}{2}\frac{1}{2})$ beams always split along either [10] or [01] so that the domain boundaries do not cross each other. As discussed below, structures having unit cell with C_{2v} symmetry may have two types of antiphase boundaries, associated with different defect (domain wall) energies. One of the boundary types will therefore be formed preferentially, producing long thin domains in agreement with the observations.

Figures 11(a) and 11(b) illustrate the intensity variation for structures with displacements perpendicular and parallel to the superlattice vector, respectively, The observed $I(\mathbf{k})$ dependence follows the trend shown in Fig. 11(a), and the direction of **d** is therefore known. However, the patterns do not permit a distinction between the pure harmonic PLD and the antiphase domain descriptions since satellites with $n > 1$ have never been seen for W(100)/H [although they are present in the case of Mo(100)/H].[10]

V. INCOMMENSURATE STRUCTURES

The splitting of the half-order beams shows that the surface periodicity changes continuously when θ exceeds $\approx \frac{1}{3}$. As discussed above, the new periodicities could be due to periodic lattice distortions of different harmonic content, including antiphase domains having a $(\sqrt{2} \times \sqrt{2})$ unit cell. Although the diffraction patterns are similar, the structures are distinctly different on a local atomic scale. For instance, in the harmonic PLD structure with $\mathbf{q} = [(1-\Delta)(\pi/a), \pi/a]$, the magnitude of the atomic displacements varies slowly across the surface; in the antiphase structure, on the other hand, the magnitude of the atomic displacement is constant throughout. The main characteristics to be explained by either model are the continuous nature of the splitting, the detailed dependence of the degree of splitting on the temperature and the coverage, and the fact that the $(\frac{1}{2}\frac{1}{2})$ beams split along [10] and [01].

The finite negative slope of the line dividing the $(\sqrt{2} \times \sqrt{2})$ and the incommensurate phases in Fig. 2 shows that the beam splitting is both coverage and temperature dependent. Extrapolation of this line suggests that a $T = 0$ the onset of beam splitting would occur near $\theta = \frac{1}{2}$. The temperature dependence of the beam splitting 2Δ at a fixed coverage is plotted against temperature in Fig. 12. The data were derived from photographs taken

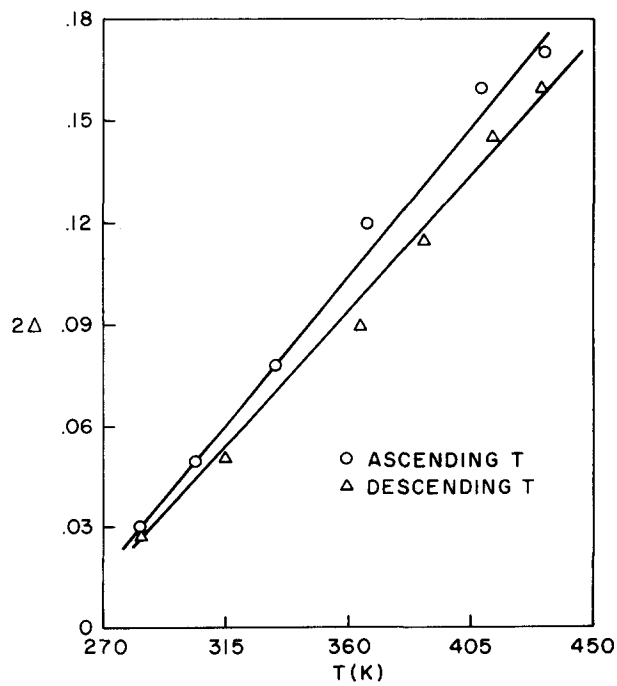

FIG. 12. The splitting 2Δ of the half-order beams as a function of temperature measured as a function of increasing (circles) and decreasing (triangles) T.

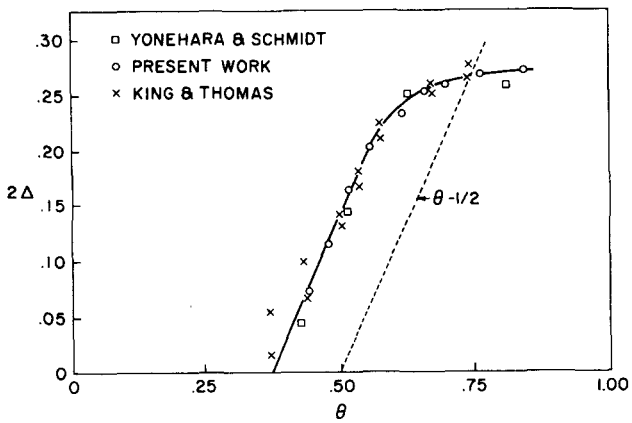

FIG. 13. The splitting 2Δ of the half-order beams as a function of coverage. The broken line is the function $2\Delta = \theta - 0.5$.

about 10 s apart as the temperature was changed. In one run in Fig. 12, the data were taken in order of increasing temperature and the beams are seen to split further from photo to photo. The other run was made as the temperature was lowered to verify that the measured change was due to the temperature and not to a slight further adsorption of hydrogen.

The coverage dependence of Δ near room temperature is shown in Fig. 13. Data from the present work and from two other studies[14,35] are shown; they have been normalized so that the initial splitting occurs at the same coverage $\theta = \frac{1}{3}$. As seen, through most of this region of the phase diagram, Δ increases approximately linearly with θ and the slope is near unity. The maximum value of 2Δ is slightly less than $\frac{1}{3}$. At lower temperatures the curve in Fig. 13 would approach the $(\theta - \frac{1}{2})$ line, as suggested by the phase diagram in Fig. 2.

To explain the H/W(001) behavior in terms of an antiphase domain model, it may be assumed that the surface is made up of $(\sqrt{2}\times\sqrt{2})$ unit cells having C_{2mm} symmetry and distortions along $\langle 10\rangle$. Antiphase boundaries divide the surface into domains. A distribution of domain sizes[32] will cause the $n>1$ satellites to be weak so that a $(\frac{1}{2}\frac{1}{2})$ beam splits into only two new beams. The magnitude of the splitting will be inversely proportional to the average domain size, and the width of the individual beams will be related to the width of the domain size distribution.

As illustrated in Fig. 14, the surface can have two distinct types of domain boundary ("wall"), the atomic displacements being either parallel to or perpendicular to the boundary, and in general these will give different wall energies. To account for the domain selection, the domain walls must be oriented preferentially across rather than along the terrace. If the domain walls are considered as defects, the qualitative temperature dependence can be explained, since a larger number of defects will be present at higher temperatures, producing smaller domains and hence increasing the beam splitting.

The coverage dependence of the beam splitting suggests that excess hydrogen, above a certain coverage, is associated with the domain walls. The splitting would vary as $(\theta - \frac{1}{2})$ if the hydrogen first induced a perfect $(\sqrt{2}\times\sqrt{2})$, which would be complete at $\theta = \frac{1}{2}$, and if then each additional adatom (per W atom row) gave rise to a new domain boundary. The offset of the $2\Delta(\theta)$ curve (see Fig. 13) to lower coverage could be due to the finite temperature of the system. [General theoretical consideration[36,37] of the domain wall interaction energy suggest a power-law dependence of the splitting on both T and θ, i.e., $\Delta \propto (\theta - \theta_0)^\alpha \propto (T - T_0)^\alpha$; however, for a related model system the value of α was found to be $\frac{1}{2}$ rather than 1.]

The fact that the beams split along $\langle 10\rangle$ and not in some arbitrary direction is easily rationalized by the antiphase model since the walls are expected to be parallel to one of the symmetry axes of the substrate. Finally, in an antiphase model the beams are not expected to split beyond $2\Delta = \frac{1}{3}$ because at this point the identity of the $(\sqrt{2}\times\sqrt{2})$ units is destroyed. Thus, all of the LEED observations on the incommensurate structures can be rationalized by this model.

As an alternative model, the incommensurate structure is assumed to arise from a distortion wave with few or no higher harmonics. Such a modulation of the lattice would imply CDW formation accompanied by the softening of a surface phonon, and the periodicity is expected to depend directly on the Fermi wave vector, i.e., $q = 2k_F$.[12] The relationship of the PLD/CDW structures to the surface band structure of W(001) and Mo(001) has been discussed elsewhere[10,12,13] and this mechanism appears plausible at least for the clean surface rearrangement. However, it is not clear that the mechanism also can explain the structural changes observed when hydrogen is present. The effects of θ and T on the shape of the $2D$ Fermi surface are not known, so the behavior shown in Figs. 12 and 13 does not provide even a qualitative test. However, it would seem to be a remarkable coincidence if changes in k_F alone could cause the $(\frac{1}{2}\frac{1}{2})$ splitting to proceed precisely in the $\langle 10\rangle$ directions.[38] This feature is more likely to be a consequence of the adatom bonding geometry. Therefore, any model based exclusively on a band picture will probably turn out to be inadequate.

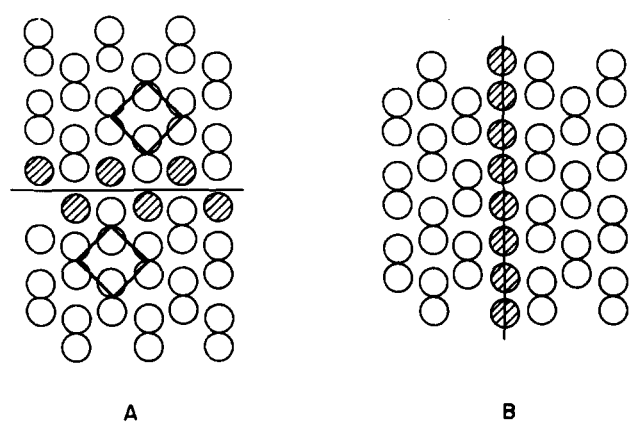

FIG. 14. Models of antiphase boundaries. In (A) the domain wall is perpendicular to the substrate atom displacements; in (B) the wall is parallel to the displacements. The bonding of the shaded atoms differs from that of the atoms in the perfect structure. The H atoms are not shown. (A) appears to be the favored structure.

VI. CONSEQUENCES OF SUBSTRATE REARRANGEMENT

The occurrence of substrate rearrangement in H/W(001) offers an explanation not only for the LEED observations but also for a number of other phenomena which cannot be understood in terms of the lattice gas (LG) model.[38] In that model the substrate is assumed to provide a rigid assembly of adsorption sites with fixed properties, and the coverage-dependent changes of the surface are ascribed to indirect adatom–adatom interactions.

The thermal desorption kinetics and the electron-stimulated desorption (ESD) yield illustrate the failure of the LG model for H/W(001). Lateral H–H interactions could cause the drop seen in the desorption energy E_d at $\theta \approx 0.5$,[7] but they would also be expected to produce an additional drop near $\theta = 1$ when H atoms are forced to occupy adjacent sites along ⟨11⟩. This second drop is not observed.[7,20] The ESD yield as a function of coverage shows a pronounced maximum[17] which has been attributed to a conversion of the adsorbed H atoms from on-top to bridge sites.[39] However, ELS[40] shows that the H atoms occupy bridge sites at all coverages.

A model that includes a rearrangement of the substrate gives a quite different picture of the surface.[38] The existence of a PLD means that the adatom–substrate interaction must vary across the surface at any given coverage, and both the period and the amplitude of this distortion change as the coverage (and/or the temperature) changes. The observed variation in the desorption energy and in the ESD yield are among the expected consequences of these changes in the substrate structure.

ACKNOWLEDGMENTS

This work was supported by the Brown University Materials Sciences Program, funded by the National Sciences Foundation, and by Grant No. NSF-DMR 79-24396.

[1]L. D. Schmidt, in *Interactions on Metal Surfaces*, edited by R. Gomer (Springer, New York, 1975), p. 63.
[2]E. W. Plummer, in *Interactions on Metal Surfaces*, edited by R. Gomér (Springer, New York, 1975), p. 143.
[3]T. E. Felter, R. A. Barker, and P. J. Estrup, Phys. Rev. Lett. **38**, 1138 (1977).
[4]M. K. Debe and D. A. King, J. Phys. C **10**, L303 (1977).
[5]M. K. Debe and D. A. King, Phys. Rev. Lett. **39**, 708 (1977).
[6]R. A. Barker, P. J. Estrup, F. Jona, and P. M. Marcus, Solid State Commun. **25**, 375 (1978).
[7]R. A. Barker and P. J. Estrup, Phys. Rev. Lett. **41**, 1307 (1978).
[8]M. R. Barnes and R. F. Willis, Phys. Rev. Lett. **41**, 1727 (1978).
[9]I. Stensgaard, L. C. Feldman, and P. J. Silverman, Phys. Rev. Lett. **42**, 247 (1979); I. Stensgaard and L. C. Feldman, Surf. Sci. **87**, 410 (1979).
[10]P. J. Estrup, J. Vac. Sci. Technol. **16**, 635 (1979).
[11]R. A. Barker, S. Semancik, and P. J. Estrup, Surf. Sci. **94**, L162 (1980).
[12]E. Tosatti, Solid State Commun. **25**, 637 (1978); E. Tosatti in Karpacz Winter School of Theoretical Physics (to be published).
[13]J. E. Inglesfield, J. Phys. C **11**, L69 (1978); H. Krakauer, M. Posternak, and A. J. Freeman, Phys. Rev. Lett. **43**, 1885 (1979).
[14]D. A. King and G. Thomas, Surf. Sci. **92**, 201 (1980).
[15]P. J. Estrup and J. Anderson, J. Chem. Phys. **45**, 2254 (1966).
[16]R. A. Barker, T. E. Felter, S. Semancik, and P. J. Estrup, J. Vac. Sci. Technol. **17**, 755 (1980).
[17]T. E. Madey, Surf. Sci. **36**, 287 (1973); T. E. Madey and J. T. Yates, Jr., in *Structures et Propriétes des Surfaces des Solides* (CNRS, Paris, 1970), No. 187, p. 155.
[18]See Refs. 1, 9, 14, and 17.
[19]T. E. Felter and P. J. Estrup, Appl. Surf. Sci. **1**, 120 (1977).
[20]R. A. Barker and P. J. Estrup (to be published).
[21]G.-C. Wang, T.-M. Lu, and M. G. Lagally, J. Chem. Phys. **69**, 479 (1978).
[22]A. R. Kortan, P. I. Cohen, and R. L. Park, J. Vac. Sci. Technol. **16**, 541 (1979); T. D. Roelofs, R. L. Park, and T. L. Einstein, *ibid.* **16**, 478 (1979).
[23]See, for example, I. Als-Nielsen, in *Phase Transitions and Critical Phenomena*, edited by C. Domb and M. S. Green (Academic, New York, 1976), Vol. 5a, p. 87.
[24]K. H. Lau and S. C. Ying, Phys. Rev. Lett. **44**, 1222 (1980).
[25]M. K. Debe and D. A. King, Surf. Sci. **81**, 193 (1979).
[26]P. Heilmann, K. Heinz, and K. Müller, Surf. Sci. **89**, 84 (1979); K. Müller (private communication).
[27]J. A. Walker, M. K. Debe, and D. A. King (to be published).
[28]A. Fasolini, G. Santoro, and E. Tosatti, Phys. Rev. Lett. **44**, 1684 (1980).
[29]P. Bak, Solid State Commun. 32, 581 (1979).
[30]A. J. Melmed, R. T. Tung, W. R. Graham, and G. D. W. Smith, Phys. Rev. Lett. **43**, 1521 (1979). No lateral displacements are seen in the FIM images, as also reported by T. T. Tsong and J. Sweeney, Solid State Commun. **30**, 767 (1979).
[31]R. W. James, *The Optical Principles of the Diffraction of X-Rays* (Bell, London, 1965).
[32]J. E. Houston and R. L. Park, Surf. Sci. **21**, 209 (1970).
[33]G. Ertl and J. Küppers, Surf. Sci. **21**, 61 (1970).
[34]W. P. Ellis and B. P. Campbell, Trans. Am. Crystallogr. Assoc. **4**, 97 (1968).
[35]K. Yonehara and L. D. Schmidt, Surf. Sci. **25**, 238 (1971).
[36]V. L. Pokrovsky and A. L. Talapov, Phys. Rev. Lett. **42**, 65 (1979).
[37]S. C. Ying (private communication).
[38]P. J. Estrup and R. A. Barker, in *Ordering in Two Dimensions*, edited by S. Sinha (North-Holland, New York, 1980), p. 39.
[39]R. Jaeger and D. Menzel, Surf. Sci. **63**, 232 (1977).
[40]W. Ho, R. F. Wallis, and E. W. Plummer, Phys. Rev. Lett. **40**, 1463 (1978).